PCCP

PAPER

Cite this: Phys. Chem. Chem. Phys., 2014, 16, 2928

Theoretical and experimental studies of the interactions between Au_2^- and nucleobases†

Guo-Jin Cao,[ab] Hong-Guang Xu,[a] Wei-Jun Zheng*[a] and Jun Li*[b]

Received 23rd October 2013, Accepted 29th November 2013

DOI: 10.1039/c3cp54478h

www.rsc.org/pccp

Combined anion photoelectron spectroscopy and relativistic quantum chemical studies are conducted on nucleobase–Au_2^- cluster anions. The vertical detachment energies of uracil–Au_2^- (UAu_2^-), thymine–Au_2^- (TAu_2^-), cytosine–Au_2^- (CAu_2^-), adenine–Au_2^- (AAu_2^-), guanine–Au_2^- (GAu_2^-) are determined to be 2.71 ± 0.08 eV, 2.74 ± 0.08 eV, 2.67 ± 0.08 eV, 2.65 ± 0.08 eV and 2.73 ± 0.08 eV, respectively, based on the measured photoelectron spectra. Through computational geometry optimizations we have identified the lowest-energy structures of these nucleobase–Au_2^- cluster anions. The structures are further confirmed by comparison of theoretically calculated vertical and adiabatic electron detachment energies with experimental measurements. The results reveal that the Au_2^- anion remains as an intact unit and interacts with the nucleobases through N–H···Au or C–H···Au *nonconventional hydrogen bonds*. The nucleobase–Au_2^- cluster anions have relatively weak N–H···Au hydrogen bonds and strong C–H···Au hydrogen bonds compared to those of nucleobase–Au^- anions.

Introduction

The unusually strong interactions between gold and DNA have attracted tremendous attention because of their importance in biology, medicine, and nanotechnology.[1–3] Generally, due to significant relativistic effects,[4–6] gold tends to show a unique covalence in bonding with soft Lewis bases.[6–11] Particularly, gold nanoparticles can be stabilized by thiol-derivative monolayers and the adsorptions are mainly dominated by the interactions between Au and thiolate. However, Herne *et al.* found that non-thiolated single-stranded DNA (ssDNA) could still bind to gold surfaces.[12] Experimental studies have also shown that DNA bases interact with gold clusters in a complex and sequence-dependent manner.[13–15] Consequently, the interactions of gold clusters with DNA bases play an important role in these processes. Investigation of gold–nucleobase interactions in detail can provide insight into the interactions of gold with DNA and help to find potential applications of gold clusters and nucleobase complexes.[16]

Many experiments have been conducted to study the interactions of nucleobases with gold surfaces and gold nanoparticles in condensed phases.[15,17–22] However, experimental studies of the interactions between gold clusters and nucleobases in the gas phase are rather scarce. In order to understand the nature of nucleobase–gold interactions, it is necessary to investigate the isolated systems where the effects of the environments are absent. Gas-phase studies on the nucleobase–gold interactions can be used as an alternative approach to help the understanding of the mechanism of gold clusters binding to nucleobases.

On the other hand, a number of gold–nucleobase compounds were studied theoretically in recent years.[16,23–37] Kryachko *et al.*[25] investigated the interactions of Au_3 and Au_4 neutral clusters with DNA bases and found that the most stable planar complexes were formed *via* N–H···Au or O–H···Au nonconventional hydrogen bonds (NCHB). Recently, Martinez[35] carried out a density functional theory (DFT) study on the interactions between nucleobases and neutral gold clusters of up to 20 Au atoms. They found that the gold clusters with an odd number of atoms and planar structures have better donor–acceptor properties. These characteristics of gold clusters were also confirmed by other researchers.[37] The NCHB features were also found in the interactions of metal ions and small clusters of Cu, Ag and Au with pterins.[38]

In our preceding paper, we provided the experimental evidence for the existence of NCHBs in the nucleobase–gold complexes and found that the gold anion can stabilize certain tautomers of nucleobases.[39] In order to help the understanding of the nucleobase–Au_2^- interactions, here we carried out a joint photoelectron spectroscopy (PES) and DFT study on the nucleobase–Au_2^- complexes. The vertical and adiabatic electron detachment energies are measured experimentally along with the PES spectra. The geometries of the anions are determined through DFT calculations with scalar relativistic (SR) and spin–orbit (SO) coupling effects.

---

[a] Beijing National Laboratory for Molecular Sciences & State Key Laboratory of Molecular Reaction Dynamics, Institute of Chemistry, Chinese Academy of Sciences, Beijing 100190, China. E-mail: zhengwj@iccas.ac.cn; Fax: +86 62563167

[b] Department of Chemistry and Key Laboratory of Organic Optoelectronics and Molecular Engineering of Ministry of Education, Tsinghua University, Beijing 100084, China. E-mail: junli@mail.tsinghua.edu.cn; Fax: +86 62797472

† Electronic supplementary information (ESI) available. See DOI: 10.1039/c3cp54478h

Experimental details

The experiment was conducted on a home-built apparatus consisting of a time-of-flight mass spectrometer and a magnetic-bottle photoelectron spectrometer, as described elsewhere.[40] The UAu_2^-, TAu_2^-, CAu_2^-, AAu_2^- and GAu_2^- cluster anions were produced by laser vaporization of rotating and translating disk targets with the second harmonic (532 nm) of a nanosecond Nd:YAG laser (Continuum Surelite II-10). Each disk target was prepared by pressing a powder mixture of gold (99.99%) and nucleobase (uracil, Alfa Aesar, >99%; thymine, Alfa Aesar, 97%; cytosine, Sigma-Aldrich, 99%; adenine, Sigma-Aldrich, 99%; guanine, Alfa Aesar, >98%) at a molar ratio of 1 : 2. Helium gas with a backing pressure of 5.5 atm was delivered through a pulsed valve into the laser ablation source to cool the formed cluster anions. These cluster anions were mass-selected and photodetached with 266 nm or 193 nm photons. The resultant electrons were energy-analyzed by the magnetic-bottle photoelectron spectrometer. The photoelectron spectra were calibrated using the spectra of Cu^- and Au^- taken at similar conditions. The resolution of the photoelectron spectrometer was approximately 40 meV for electrons with 1 eV kinetic energy.

Computational details

The calculations of UAu_2^-, TAu_2^-, CAu_2^-, AAu_2^- and GAu_2^- cluster anions were performed with the Gaussian 09 program package[41] using the B3LYP[42,43] density functional method. The all-electron 6-31++G(d,p) basis sets were used for the atoms in the nucleobases, and the Lanl2dz basis set and associated effective core potential (ECP) were used for gold during the optimization calculations. We tested the theoretical method used by calculating the bond length of Au_2 and compared the result with the experimental measurements. The result obtained using the B3LYP functional with the Lanl2dz basis set is in good agreement with the experimental data in the literature.[44] Estrin *et al.*[45] confirmed that the structures, relative energies, and vibrational frequencies of the tautomers of uracil and thymine calculated by using local and gradient-corrected density functionals agree well with the experimental results. Sambrano *et al.*[46] conducted a theoretical study on the tautomers of cytosine using hybrid B3LYP with the 6-31++G(d,p) basis set and found that the calculated results were consistent with the experimental data. Therefore, B3LYP/6-31++G(d,p)$\cup$Lanl2dz is suitable for the calculation of nucleobase–Au_2^- cluster anions. The predominant tautomers of the nucleobase were taken into account in the search for low-energy isomers of these complexes. No symmetry constraint was imposed during the geometry optimizations. The vibrational frequencies were calculated to confirm that their structures are real local minima. The natural bond orbital (NBO)[47,48] analyses of the nucleobase–Au_2 clusters were also performed at B3LYP/6-31++G(d,p)$\cup$Lanl2dz to gain insights into the charge distributions of the nucleobase–Au_2^- cluster anions. The zero-point energy (ZPE) corrections were included for all the calculated energies. To further understand the nature of the NCHBs in these gold cluster–nucleobase complexes, we also performed topological analysis by means of Bader's atoms in molecules (AIM) theory[49,50] to calculate the electron density, the Laplacian of the electron density at the bond critical points (BCP). The topological analysis was carried out using Multiwfn 2.6.1 package.[51]

To investigate the spin–orbit (SO) coupling effects on the VDE energies for these open shell complexes, density functional calculations were carried out on the neutral and negatively charged Au_2–nucleobase clusters using Amsterdam Density Functional program (ADF 2012.01).[52–54] In these calculations, the generalized gradient approximation (GGA) of the Perdew–Wang exchange–correlation functional (PW91) was employed. The uncontracted Slater basis sets with the quality of triple-zeta plus two polarization functions (TZ2P) were used, with the frozen core approximation applied to the $[1s^2–4f^{14}]$ core for Au, and the $[1s^2]$ cores for C, N and O. The scalar relativistic (SR) and SO coupling effects on the VDEs of Au_2–nucleobase$^-$ cluster anions were taken into account by the zero-order-regular approximation (ZORA). The geometries were optimized at the SR level and the single-point energy calculations were performed at the SR and SO level.

Results and discussion

The photoelectron spectra of UAu_2^-, TAu_2^-, CAu_2^-, AAu_2^- and GAu_2^- cluster anions obtained with 266 nm and 193 nm photons are shown in Fig. 1. The adiabatic detachment energies (ADEs) and vertical detachment energies (VDEs) of nucleobase–Au_2^- anions determined from the PES spectra are summarized in Table 1. The PES spectra of UAu_2^-, TAu_2^-, CAu_2^-, AAu_2^- and GAu_2^- with 266 nm photons are each dominated by a single peak centered at 2.71 eV, 2.74 eV, 2.67 eV, 2.65 eV and 2.73 eV, respectively. The shift between the VDE of UAu_2^- and that of Au_2^- is 0.70 eV. Similarly, for the first peaks in the spectra of TAu_2^-, CAu_2^-, AAu_2^- and GAu_2^-, the shifts are 0.73, 0.66, 0.64 and 0.72 eV, respectively, relative to that of Au_2^-. The spectra of nucleobase–Au_2^- taken with 193 nm photons are characterized by a small peak at the low electron binding energy side and very strong features at the high electron binding energy side, resembling the photoelectron spectrum of Au_2^-.[55] It indicates that the neutral nucleobase–Au_2 complexes have very large HOMO–LUMO gaps. The spectrum of UAu_2^- taken with 193 nm photons has a sharp peak centered at 2.71 eV, a small shoulder centered at 4.33 eV, a broad feature centered at 4.53 eV, followed by a small peak centered at 4.85 eV and three unresolved peaks centered at 5.41 eV, 5.66 eV and 5.74 eV. The spectrum of TAu_2^- contains a sharp peak centered at 2.74 eV, a small shoulder centered at 4.41 eV, a broad peak centered at 4.82 eV, an unresolved broad features centered at 5.58 eV. The photoelectron spectrum of CAu_2^- taken with 193 nm photons is presented with a sharp peak centered at 2.67 eV, a small shoulder centered at 4.16 eV, a broad peak centered at 4.67 eV and an unresolved broad feature centered at 5.41 eV. The spectrum of AAu_2^- contains a sharp peak centered at 2.65 eV, and three small shoulders centered at 4.32 eV, 4.65 eV and 4.93 eV, followed by a broad feature at higher binding energy.

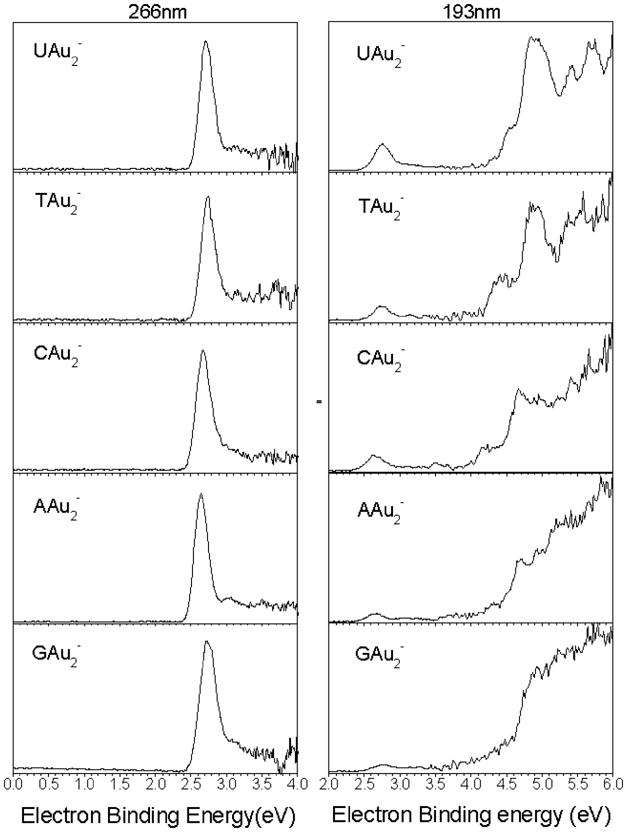

Fig. 1 Photoelectron spectra of nucleobase–Au_2^- anions recorded with 266 nm and 193 nm photons.

Table 1 Experimental VDEs and ADEs of the nucleobase–Au_2^- complexes measured from their photoelectron spectra[a]

	VDE	ADE
UAu_2^-	2.71(8)	2.54(8)
TAu_2^-	2.74(8)	2.54(8)
CAu_2^-	2.67(8)	2.48(8)
AAu_2^-	2.65(8)	2.46(8)
GAu_2^-	2.73(8)	2.52(8)

[a] All the energies are in eV. The numbers in parentheses indicate the uncertainties in the last digit.

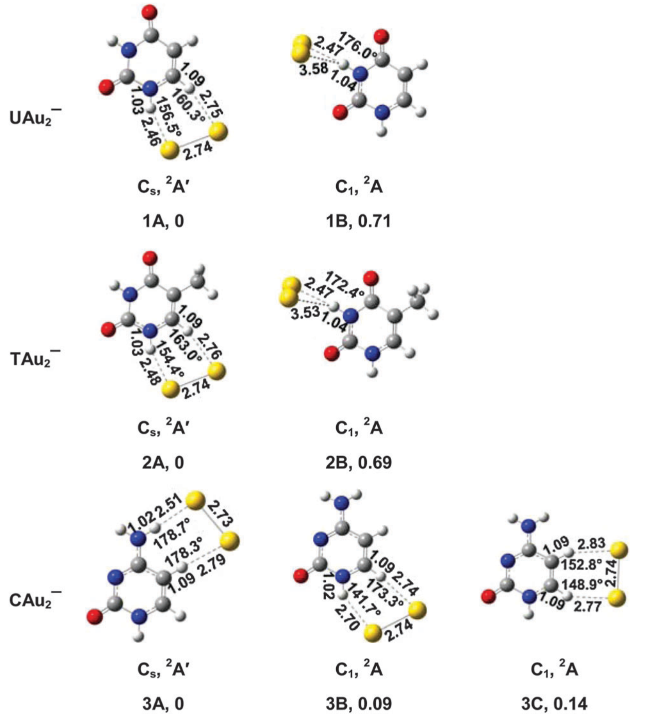

Fig. 2 Structures and relative energies of the low-lying isomers of uracil–Au_2^-, thymine–Au_2^- and cytosine–Au_2^- (all the energies are in eV). The bond distances are in angstroms and the bond angles are in degrees.

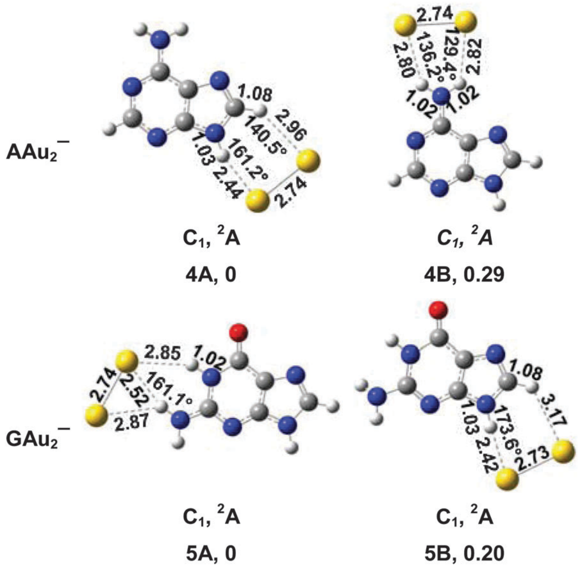

Fig. 3 Structures and relative energies of the low-lying isomers of adenine–Au_2^- and guanine–Au_2^- anions (all the energies are in eV). The bond distances are in angstroms and the bond angles are in degrees.

The spectrum of GAu_2^- contains a small peak centered at 2.73 eV, followed by a broad feature at higher binding energy. The spectra of AAu_2^- and GAu_2^- are less resolved than those of UAu_2^-, TAu_2^-, and CAu_2^- most likely due to their more complex structures and the existence of minor low-lying isomers.

We have searched various possible structures for these nucleobase–Au_2^- anions, including nucleobases binding Au_2 or two Au atoms at different positions. The optimized structures, VDEs, and ADEs of nucleobase–Au_2^- with all the tautomers of nucleobases are listed in Tables S1–S5 (ESI†). The optimized structures of the typical low-lying isomers of UAu_2^-, TAu_2^-, CAu_2^-, AAu_2^- and GAu_2^- are shown in Fig. 2 and 3. The calculated relative energies, VDEs, ADEs, and natural charges from NBO analyses of these isomers are summarized in Table 2. The VDEs were obtained based on the energy difference between the neutral and anion clusters at the ground state geometry of the anion.

UAu_2^-, TAu_2^-, and CAu_2^-

As can be seen in Fig. 2, the lowest-lying isomer **1A** of UAu_2^- has a planar structure with C_s symmetry. The structure of

Table 2 Relative energies, VDEs and ADEs of the low-energy isomers of nucleobase–Au_2^- anions obtained by DFT calculations. The basis set 6-31++g(d,p) for C, N, O, H, and Lanl2dz for Au were used

	Isomers	ΔE (eV)	Symmetry	State	Natural charge		ADE (eV)		VDE (eV)	
					Au(1)	Au(2)	Theo.	Expt.	Theo.	Expt.
UAu_2^-	**1A**	0.00	C_s	$^2A'$	−0.45	−0.46	2.25	2.54	2.91	2.71
	1B	0.71	C_1	^2A	−0.46	−0.48	1.53		2.24	
TAu_2^-	**2A**	0.00	C_s	$^2A'$	−0.45	−0.46	2.19	2.54	2.88	2.74
	2B	0.69	C_1	^2A	−0.46	−0.48	1.51		2.24	
CAu_2^-	**3A**	0.00	C_s	$^2A'$	−0.45	−0.48	2.67	2.48	2.84	2.67
	3B	0.09	C_1	^2A	−0.47	−0.48	1.83		2.74	
	3C	0.14	C_1	^2A	−0.48	−0.49	2.54		2.71	
AAu_2^-	**4A**	0.00	C_1	^2A	−0.46	−0.47	2.57	2.46	2.75	2.65
	4B	0.29	C_s	$^2A'$	−0.49	−0.49	2.34		2.48	
GAu_2^-	**5A**	0.00	C_1	^2A	−0.44	−0.47	2.09	2.52	2.94	2.73
	5B	0.20	C_1	^2A	−0.45	−0.47	2.57		2.74	

isomer **1A** from our calculations is consistent with theoretical calculations conducted by Martinez.[56] Isomer **1A** is formed by attaching the Au_2 cluster preferentially to the 2,4-diketo tautomer of uracil at N1–H and C6–H. The Au–Au distance (2.74 Å) in isomer **1A** is close to the Au–Au bond length in the isolated Au_2 cluster anion unit, indicating that the Au_2^- anion unit maintains its structure in the nucleobase–Au_2^- cluster anions. The VDE of isomer **1A** is calculated to be 2.91 eV at the B3LYP/6-31++G(d,p)∪Lanl2dz level, which is in reasonable agreement with the experimental value (2.71 eV) considering the relatively small basis sets and approximate exchange–correlation functional used. The N1–H···Au angle in **1A** is about 156.5° and the C6–H···Au angle is about 160.3°. The N1–H bond is elongated by 0.02 Å and the C6–H bond is elongated by 0.01 Å relative to those of the uracil monomer. In the isomer **1B**, the Au_2^- cluster preferentially binds to the uracil at O7–H and N3–H. This isomer is 0.71 eV higher in energy than isomer **1A** and its theoretical VDE (2.24 eV) is much lower than the experimental value. Considering the optimized total energies and the agreement of the VDEs, we conclude that isomer **1A** is the most stable isomer detected in our experiments.

The isomers of TAu_2^- can be considered as derived from the isomers of UAu_2^- by attaching a CH_3 group to the C5 atom of uracil. The lowest-lying isomer **2A** of TAu_2^- has a C_s symmetry. The VDE of isomer **2A** is calculated to be 2.88 eV, in good agreement with the experimental value (2.74 eV). Similar to isomer **1A**, the N1–H···Au and C6–H···Au angles of isomer **2A** are about 154.4° and 163.0°, respectively. The N1–H bond is elongated by 0.04 Å relative to that of the thymine monomer, and the C6–H bond is elongated by 0.01 Å compared to that of the isolated thymine. The isomer **2B** is less stable than isomer **2A** by 0.69 eV. Its theoretical VDE is calculated to be 2.24 eV, which does not match with the experimental values well. Therefore, the existence of isomer **2B** in the experiments can be ruled out; isomer **2A** corresponds to the major peaks observed in the spectrum of TAu_2^-.

Fig. 2 shows three low-lying isomers of CAu_2^-. They lie close in energy, with the energy difference being within 0.14 eV at the B3LYP level of calculations. We also performed single-point MP2 calculations of the isomers **3A**, **3B** and **3C** of CAu_2^- using Lanl2dz and 6-31++g(d,p) basis sets; the relative energies are 0.00, 0.06, 0.13 eV, respectively, similar to the DFT results. The lowest-lying isomer **3A** of CAu_2^- formed by the interactions of the Au_2^- anion with the N8–H and C5–H bonds of the amino-oxo-N1H tautomer has a planar structure with C_s symmetry. The N8–H···Au and C5–H···Au units have nearly linear arrangements (∠N8–H···Au = 178.7°, ∠C5–H···Au = 178.3°). Both N8–H and C5–H bonds are elongated by 0.01 Å relative to those of the cytosine monomer. Isomer **3B** has the Au_2^- anion interacting with the N1–H and C6–H bonds of cytosine. Isomer **3C** is formed by attaching the Au_2^- anion to the C5–H and C6–H bonds of cytosine. We note that isomer **3C** contains two sets of C–H···Au interactions. The calculated VDEs of isomers **3A**, **3B** and **3C** are 2.84, 2.74 and 2.71 eV, respectively, which are all close to the experimental measurements. It is likely that isomer **3A** is the most probable isomer in the experiments, while the existence of isomers **3B** and **3C** cannot be completely ruled out.

AAu_2^- and GAu_2^-

As seen in Fig. 3, the lowest-energy isomer **4A** of AAu_2^- has a nonplanar structure with C_1 symmetry. The lowest-lying isomer **4A** is formed by attaching the Au_2^- anion to the C8–H and N9–H of the canonical tautomer, similar to the structure of AAu_2^- calculated by Martinez.[56] In the planar structure of isomer **4B**, two sets of N–H···Au groups are formed when the Au_2^- anion interacts with the two N10–H bonds of adenine. The calculated VDE and ADE of isomer **4A** are 2.75 eV and 2.57 eV, respectively, in good agreement with the experimental values (2.65 eV and 2.46 eV). Although the calculated VDE of isomer **4B** (2.48 eV) is close to the experimental measurement, isomer **4B** is higher than isomer **4A** by 0.29 eV in energy, indicating that isomer **4A** is the most probable isomer in the experiment.

The two low-lying isomers **5A** and **5B** of GAu_2^- both have nonplanar structures with C_1 symmetry. Isomer **5A** can be considered as the Au_2^- anion interacts with the N1–H and N10–H bonds of the K–N9H tautomer of guanine. The theoretical VDE (2.94 eV) of isomer **5A** agrees with the experimental value (2.73 eV) estimated from the first strong peak in the spectrum of GAu_2^- (Fig. 1). In isomer **5B**, the gold cluster anion interacts with C8–H and N9–H of the canonical tautomer of guanine. While the theoretical VDE of isomer **5B** (2.74 eV) is in reasonable agreement with the experimental value, isomer **5B** is less stable than the lowest-energy isomer **5A** by 0.20 eV. So isomer **5A** is the most probable isomer detected in our experiment.

Gold has large relativistic effects, which significantly increase the relativistic stabilization and contraction of the 6s shell.[4–6] The relativistic effects mainly consist of SR and SO coupling effects. The reduced 6s–5d energy gap due to relativistic effects leads to hybridization of the atomic s–d levels and overlap of the 5d shells of adjacent atoms in the cluster, thus resulting in a high stability of the Au$_n$ cluster.[57–62] In order to investigate the SO coupling effects on nucleobase–Au$_2^-$ cluster anions, we also performed theoretical calculations with inclusion of the SO relativistic effects using the ADF 2012.01 program.[52–54] These VDEs calculated at SR and SO are summarized in Table 3. All the differences in energies between the VDEs computed at SR and the corresponding VDEs calculated at SO for the most probable isomers are within 0.02 eV, indicating that the SO coupling effects have little influence on the VDEs for nucleobase–Au$_2^-$ anions. Our analysis shows that the HOMO of UAu$_2^-$ (**1A**) only contains 4.8% Au 5d and 9.2% Au 6p characters. It results in less SO splitting for UAu$_2^-$ since the SO coupling effects are mainly from the Au 5d and Au 6p orbitals. The differences between the VDEs calculated at SR and SO are very small, indicating that the above-mentioned comparison between experimental values and theoretical results computed at the SR level *via* Gaussian package is valid. To further make certain the accuracy of the methods used, the VDE of UAu$_2^-$ (**1A**) was calculated using B3LYP/6-31++G(d,p)∪Lanl2dz, B3LYP/aug-cc-pVTZ∪aug-cc-pVTZ-PP, DFT-D[63,64]/TZ2P, and CAMY-B3LYP[65]/TZ2P calculations. These calculations were implemented in ADF2013.01[52–54] and the results are given in Table 4. The first VDE calculated at B3LYP/6-31++G(d,p)∪Lanl2dz level is slightly larger when compared with the DFT-D and CAMY-B3LYP results. We also note that the different basis sets do not show a significant effect on the calculated VDE of nucleobase–Au$_2^-$ cluster anions.

As can be seen in Fig. 2 and 3, and Table 2, the similarities in both structures and bonding of the low-lying isomers of nucleobase–Au$_2^-$ are clearly shown. In these isomers, the Au$_2^-$ anion unit still maintains its structure similar to the isolated Au$_2^-$ cluster anion. The N–H···Au interaction exists in all nucleobase–Au$_2^-$ complexes except for isomer **3C**. In the N–H···Au interactions of the most probable isomers, the N–H bond is elongated compared to the isolated nucleobase molecule and the H···Au distance (2.44 to 2.52 Å) is smaller than the sum of van der Waals radii of H (r_H = 1.20 Å)[66,67] and Au (r_{Au} = 1.66 Å).[68] The N–H···Au unit has a nearly linear arrangement. Besides, C–H···Au interactions also exist in some isomers of the nucleobase–Au$_2^-$ anion such as isomer **3C**. The analyses of the NBO charges show that the excess charge is mainly localized on the Au$_n$ units. The charge transfers slightly from the Au$_2^-$ to the N–H or C–H bond. Both N–H···Au and C–H···Au interactions in the most probable isomers are clearly three-center four-electron bonds (3c-4e) in nature. These are all in accordance with the prerequisites of nonconventional hydrogen bonds[24,25,69–71] and also satisfy the definition of hydrogen bonds proposed by IUPAC.[72] Therefore, the combination of the experimental results and theoretical calculations suggests that the Au$_2^-$ anion interacts with the nucleobases mainly *via* N–H···Au or C–H···Au hydrogen bonds.

Table 3 Theoretical vertical detachment energies (VDEs) of the low-energy isomers of the nucleobase–Au$_2^-$ anions calculated using the GGA/PW91 method (all the energies are in eV)

		VDE	
	Isomers	SR	SO
UAu$_2^-$	**1A**	2.88	2.90
	1B	2.22	2.24
TAu$_2^-$	**2A**	2.85	2.87
	2B	2.20	2.23
CAu$_2^-$	**3A**	2.80	2.82
	3B	2.68	2.70
	3C	2.63	2.65
AAu$_2^-$	**4A**	2.74	2.76
	4B	2.48	2.50
GAu$_2^-$	**5A**	2.91	2.93
	5B	2.73	2.75

Table 4 Theoretical vertical detachment energies (VDEs) of UAu$_2^-$ (**1A**) calculated using different methods. All the energies are in eV

	VDE					
	B3LYP/ 6-31++G(d,p)∪ Lanl2dz	B3LYP/ aug-cc-pVTZ∪ aug-cc-pVTZ-PP	DFT-D/ TZ2P		CAMY-B3LYP/ TZ2P	
			SR	SO	SR	SO
UAu$_2^-$	2.91	2.84	2.74	2.76	2.69	2.71

As seen in Table 5, the percentage of p orbital character in the σ-bonding hybrid of the N1–H7 bond and the C6–H10 bond of the UAu$_2^-$ cluster anion is less than that in the corresponding orbital hydridizations of uracil. The component of H decreases but the components of N and C increase in the bonding hybrid of the N1–H7 bond and the C6–H10 bond of UAu$_2^-$ relative to those of uracil. Kohn–Sham molecular orbital energy levels and isocontour surfaces of the frontier orbitals of UAu$_2^-$ are shown in Fig. 4 to provide a qualitative understanding of this trend. The highest occupied molecular orbital (HOMO) 30a′ from the Au$_2^-$ 4σ$_u$ orbital is mainly of Au 6s character with minor 5d contribution. The lowest unoccupied molecular orbital (LUMO) 12a″ MO mainly involves 2p characters of C, N, O, while the 11a″ MO (HOMO − 1) mainly consists of the Au 5d orbital. The coordination of nucleobase to Au$_2^-$ in the nucleobase–Au$_2^-$ cluster anions significantly stabilizes the σ$_u$ orbital of Au$_2^-$. Consequently, the HOMOs of nucleobase–Au$_2^-$

Table 5 NBO orbital hydridizations in UAu$_2^-$ (**1A**)

Complex	Bond orbital	Orbital hydridizations
Uracil	N1–H7 σ	$0.85 \times (sp^{2.47})_{N1} + 0.53 \times (s)_{H7}$
	C6–H10 σ	$0.79 \times (sp^{2.22})_{C6} + 0.62 \times (s)_{H10}$
Au$_2^-$	Au–Au σ	$0.71 \times (sp^{0.01}d^{0.12})_{Au1} + 0.71 \times (sp^{0.01}d^{0.12})_{Au2}$
UAu$_2^-$	N1–H7 σ	$0.87 \times (sp^{2.28})_{N1} + 0.50 \times (s)_{H7}$
	C6–H10 σ	$0.80 \times (sp^{2.12})_{C6} + 0.60 \times (s)_{H10}$
	Au–Au σ	$0.72 \times (sp^{0.01}d^{0.12})_{Au13} + 0.70 \times (sp^{0.01}d^{0.12})_{Au14}$

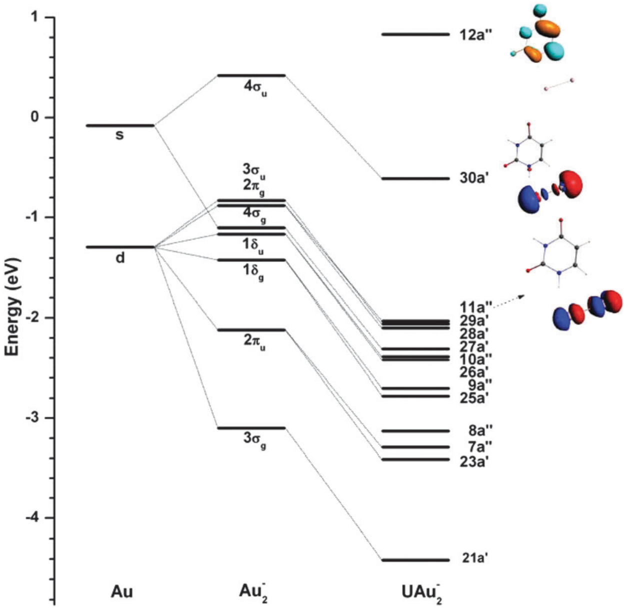

Fig. 4 Molecular orbital energy levels and isocontour surfaces (isosurface value = 0.04 au) of frontier orbitals of UAu_2^- from SR-DFT/PW91 calculation. The 30a′ orbital is singly occupied and the higher lying orbital 12a″ is unoccupied.

are much lower lying relative to the HOMO of the Au_2^- anion. These low-lying HOMOs in the nucleobase–Au_2^- anions thus have increased electron detachment energies relative to the bare Au_2^-.

The topological analysis of electron density has shown that the BCP of (3, −1) topology exists in all the N–H···Au and C–H···Au bonds of nucleobase–Au_2^-. The properties of electron density ($\rho(r)$), the Laplacian of electron density ($\nabla^2\rho(r)$), the eigenvalues of the Hessian of the electron density (λ_1, λ_2, and λ_3), and the ellipticities ($\varepsilon = \lambda_1/\lambda_2 - 1$) of the lowest-energy isomers of UAu_2^- and UAu^- calculated at the BCPs are presented in Table 6. The electron density $\rho(r)$ is above zero and in the proposed range of 0.002–0.035. The Laplacian of electron density ($\nabla^2\rho(r)$) is simply the sum of the eigenvalues λ_1, λ_2, and λ_3, above zero and in the proposed range of 0.024–0.139. These are all in accordance with the criteria for the hydrogen bonds suggested by Popelier.[73,74] A link between the electron density $\rho(r)$ and the bond strength has been suggested before.[75] As shown in Table 6, we can see that $\rho(r)$ of the N–H···Au interaction of UAu_2^- is about 0.0126, smaller than that (0.0159) of UAu^-, whereas $\rho(r)$ of the C–H···Au interaction of UAu_2^- is larger than that of UAu^-, confirming that the N–H···Au interaction in UAu_2^- is weaker than that in UAu^-, but the C–H···Au interaction in UAu_2^- is stronger than that in UAu^-. Similarly, the other nucleobase–Au_2^- complexes also have weaker N–H···Au hydrogen bonds and stronger C–H···Au hydrogen bond characteristics relative to nucleobase–Au^-. The ellipticities in the N–H···Au and C–H···Au bonds of UAu_2^- are close to zero, indicating that these bonds in nucleobase–Au_2^- mostly have σ-bonding characters. The ellipticity ε is much larger in the C–H···Au bond of UAu^-, indicating that the C–H···Au interaction has a considerable π character and is much weaker than the N–H···Au interaction in nucleobase–Au^-. The distance between a BCP and a ring critical point (RCP) also reflects structural stability. In the structure of UAu_2^-, the distance between BCP (C–H···Au) and the nearest RCP is 1.16 Å, whereas the distance between BCP (N–H···Au) and its nearest RCP is 1.22 Å, also rendering the latter as a somewhat more stable hydrogen bond. In addition, our calculations show that the binding energies of nucleobases with Au_2^- in isomers **1A**, **2A**, **3A**, **4A**, and **5A** are ∼0.57, 0.51, 0.44, 0.31 and 0.51 eV, respectively, which are much lower than those of the corresponding nucleobases–Au^-. This indicates that the sum of C–H···Au and N–H···Au interactions in nucleobase–Au_2^- is much weaker than that in nucleobase–Au^-.

Conclusions

We measured the photoelectron spectra of nucleobase–Au_2^- and investigated the structures of these clusters with density functional calculations. By comparing the calculated VDEs with the experimental measurements, the structures of nucleobase–Au_2^- anions are determined. Spin–orbit coupling does not show a significant influence on the VDEs of nucleobase–Au_2^- anions. In the nucleobase–Au_2^- cluster anions, the Au_2^- anion unit still maintains its structure similar to the isolated Au_2^- cluster anion. The bonding between nucleobase and Au_2^- cluster anion occurs mainly *via* N–H···Au or C–H···Au nonconventional hydrogen bonds. Nucleobase–Au_2^- has weaker N–H···Au hydrogen bonds and stronger C–H···Au hydrogen bond characteristics relative to nucleobase–Au^-.

Acknowledgements

This work was supported by the Natural Science Foundation of China (Grant No. 21273246). The theoretical calculations were supported by NKBRSF (Grant No. 2011CB932400) of China and were performed using an HP Itanium2 cluster at Tsinghua National Laboratory for Information Science and Technology as well as the ScGrid and Deepcomp 7000 of the Supercomputing Center, Computer Network Information Center of Chinese Academy of Sciences.

Table 6 Properties of the electron density at the bond critical points for the N–H···Au and C–H···Au bonds in UAu_2^- and UAu^-

	Bond critical point	$\rho(r)$	$\nabla^2\rho(r)$	λ_1	λ_2	λ_3	ε
UAu_2^-	N–H···Au	0.0126	0.0645	−0.0115	−0.0115	0.0874	0.0000
	C–H···Au	0.0090	0.036	−0.0072	−0.0068	0.0499	0.0640
UAu^-	N–H···Au	0.0159	0.0836	−0.0151	−0.0150	0.1137	0.0017
	C–H···Au	0.0066	0.0255	−0.0042	−0.0011	0.0309	2.8050

References

1 C. A. Mirkin, R. L. Letsinger, R. C. Mucic and J. J. Storhoff, *Nature*, 1996, **382**, 607.
2 C. A. Mirkin, *Inorg. Chem.*, 2000, **39**, 2258.
3 Y. Liu, W. Meyer-Zaika, S. Franzka, G. Schmid, M. Tsoli and H. Kuhn, *Angew. Chem., Int. Ed.*, 2003, **42**, 2853.
4 H. Schwarz, *Angew. Chem., Int. Ed.*, 2003, **42**, 4442.
5 P. Pyykkö, *Angew. Chem., Int. Ed.*, 2004, **43**, 4412.
6 L.-S. Wang, *Phys. Chem. Chem. Phys.*, 2010, **12**, 8694.
7 Y.-L. Wang, X.-B. Wang, X.-P. Xing, F. Wei, J. Li and L.-S. Wang, *J. Phys. Chem. A*, 2010, **114**, 11244.
8 H.-T. Liu, X.-G. Xiong, P. D. Dau, Y.-L. Wang, J. Li and L.-S. Wang, *Chem. Sci.*, 2011, **2**, 2101.
9 H.-T. Liu, Y.-L. Wang, X.-G. Xiong, P. D. Dau, Z. A. Piazza, D.-L. Huang, C.-Q. Xu, J. Li and L.-S. Wang, *Chem. Sci.*, 2012, **3**, 3286.
10 C.-G. Ning, X.-G. Xiong, Y.-L. Wang, J. Li and L.-S. Wang, *Phys. Chem. Chem. Phys.*, 2012, **14**, 9323.
11 H.-T. Liu, X.-G. Xiong, P. D. Dau, Y.-L. Wang, D.-L. Huang, J. Li and L.-S. Wang, *Nat. Commun.*, 2013, **4**, 2201.
12 T. M. Herne and M. J. Tarlov, *J. Am. Chem. Soc.*, 1997, **119**, 8916.
13 A. B. Steel, T. M. Herne and M. J. Tarlov, *Anal. Chem.*, 1998, **70**, 4670.
14 L. M. Demers, C. A. Mirkin, R. C. Mucic, R. A. Reynolds, R. L. Letsinger, R. Elghanian and G. Viswanadham, *Anal. Chem.*, 2000, **72**, 5535.
15 T. Boland and B. D. Ratner, *Langmuir*, 1994, **10**, 3845.
16 N. Vyas and A. K. Ojha, *Comput. Theor. Chem.*, 2012, **984**, 93.
17 N. J. Tao, J. A. DeRose and S. M. Lindsay, *J. Phys. Chem.*, 1993, **97**, 910.
18 W.-H. Li, W. Haiss, S. Floate and R. J. Nichols, *Langmuir*, 1999, **15**, 4875.
19 L. M. Demers, M. Östblom, H. Zhang, N.-H. Jang, B. Liedberg and C. A. Mirkin, *J. Am. Chem. Soc.*, 2002, **124**, 11248.
20 N. H. Jang, *Bull. Korean Chem. Soc.*, 2002, **23**, 1790.
21 H. Kimura-Suda, D. Y. Petrovykh, M. J. Tarlov and L. J. Whitman, *J. Am. Chem. Soc.*, 2003, **125**, 9014.
22 A. Gourishankar, S. Shukla, K. N. Ganesh and M. Sastry, *J. Am. Chem. Soc.*, 2004, **126**, 13186.
23 J. V. Burda, J. Sponer, J. Leszczynski and P. Hobza, *J. Phys. Chem. B*, 1997, **101**, 9670.
24 E. S. Kryachko and F. Remacle, *J. Phys. Chem. B*, 2005, **109**, 22746.
25 E. S. Kryachko and F. Remacle, *Nano Lett.*, 2005, **5**, 735.
26 A. Kumar, P. C. Mishra and S. Suhai, *J. Phys. Chem. A*, 2006, **110**, 7719.
27 P. J. Mohan, A. Datta, S. S. Mallajosyula and S. K. Pati, *J. Phys. Chem. B*, 2006, **110**, 18661.
28 P. Sharma, H. Singh, S. Sharma and H. Singh, *J. Chem. Theory Comput.*, 2007, **3**, 2301.
29 J. Valdespino-Saenz and A. Martinez, *J. Phys. Chem. A*, 2008, **112**, 2408.
30 M. K. Shukla, M. Dubey, E. Zakar and J. Leszczynski, *J. Phys. Chem. C*, 2009, **113**, 3960.
31 A. Martinez, *J. Phys. Chem. A*, 2009, **113**, 1134.
32 G. Lv, F. D. Wei, H. Jiang, Y. Y. Zhou and X. M. Wang, *THEOCHEM*, 2009, **915**, 98.
33 E. S. Kryachko, *Pol. J. Chem.*, 2009, **83**, 917.
34 J. Valdespino-Saenz and A. Martinez, *THEOCHEM*, 2010, **939**, 34.
35 A. Martinez, *J. Phys. Chem. C*, 2010, **114**, 21240.
36 G. Lv, F. D. Wei, Q. N. Li, Q. Shen, H. Jiang, Y. Y. Zhou and X. M. Wang, *J. Nanosci. Nanotechnol.*, 2010, **10**, 809.
37 W. M. Sun and R. Di Felice, *J. Phys. Chem. C*, 2012, **116**, 24954.
38 R. Vargas and A. Martínez, *Phys. Chem. Chem. Phys.*, 2011, **13**, 12775.
39 G.-J. Cao, H.-G. Xu, R.-Z. Li and W. J. Zheng, *J. Chem. Phys.*, 2012, **136**, 014305.
40 H.-G. Xu, Z.-G. Zhang, Y. Feng, J. Y. Yuan, Y. C. Zhao and W. J. Zheng, *Chem. Phys. Lett.*, 2010, **487**, 204.
41 M. J. Frisch, G. W. Trucks, H. B. Schlegel, G. E. Scuseria, M. A. Robb, J. R. Cheeseman, G. Scalmani, V. Barone, B. Mennucci, G. A. Petersson, H. Nakatsuji, M. Caricato, X. Li, H. P. Hratchian, A. F. Izmaylov, J. Bloino, G. Zheng, J. L. Sonnenberg, M. Hada, M. Ehara, K. Toyota, R. Fukuda, J. Hasegawa, M. Ishida, T. Nakajima, Y. Honda, O. Kitao, H. Nakai, T. Vreven, J. A. Montgomery Jr., J. E. Peralta, F. Ogliaro, M. Bearpark, J. J. Heyd, E. Brothers, K. N. Kudin, V. N. Staroverov, R. Kobayashi, J. Normand, K. Raghavachari, A. Rendell, J. C. Burant, S. S. Iyengar, J. Tomasi, M. Cossi, N. Rega, J. M. Millam, M. Klene, J. E. Knox, J. B. Cross, V. Bakken, C. Adamo, J. Jaramillo, R. Gomperts, R. E. Stratmann, O. Yazyev, A. J. Austin, R. Cammi, C. Pomelli, J. W. Ochterski, R. L. Martin, K. Morokuma, V. G. Zakrzewski, G. A. Voth, P. Salvador, J. J. Dannenberg, S. Dapprich, A. D. Daniels, Ö. Farkas, J. B. Foresman, J. V. Ortiz, J. Cioslowski and D. J. Fox, *Gaussian 09, Revision A.2*, Gaussian, Inc., Wallingford, CT, 2009.
42 A. D. Becke, *J. Chem. Phys.*, 1993, **98**, 5648.
43 C. Lee, W. Yang and R. G. Parr, *Phys. Rev. B: Condens. Matter Mater. Phys.*, 1988, **37**, 785.
44 B. Simard and P. A. Hackett, *J. Mol. Spectrosc.*, 1990, **142**, 310.
45 D. A. Estrin, L. Paglieri and G. Corongiu, *J. Phys. Chem.*, 1994, **98**, 5653.
46 J. R. Sambrano, A. R. de Souza, J. J. Queralt and J. Andrés, *Chem. Phys. Lett.*, 2000, **317**, 437.
47 A. E. Reed, L. A. Curtiss and F. Weinhold, *Chem. Rev.*, 1988, **88**, 899.
48 A. E. Reed and F. Weinhold, *J. Chem. Phys.*, 1983, **78**, 4066.
49 R. F. W. Bader, *Atoms in Molecules: A Quantum Theory*, Clarendon Press, Oxford, 1990, p. xviii, 438.
50 R. F. W. Bader, *J. Phys. Chem. A*, 1998, **102**, 7314.
51 T. Lu and F. Chen, *J. Comput. Chem.*, 2012, **33**, 580.
52 C. Fonseca Guerra, J. Snijders, G. Te Velde and E. Baerends, *Theor. Chem. Acc.*, 1998, **99**, 391.
53 G. te Velde, F. M. Bickelhaupt, E. J. Baerends, C. Fonseca Guerra, S. J. A. van Gisbergen, J. G. Snijders and T. Ziegler, *J. Comput. Chem.*, 2001, **22**, 931.

54 See http://www.scm.com for ADF2012.01 and ADF2013.01, SCM, Theoretical Chemistry, Vrije Universiteit, Amsterdam, The Netherlands.
55 H. Handschuh, G. Ganteför, P. S. Bechthold and W. Eberhardt, *J. Chem. Phys.*, 1994, **100**, 7093.
56 A. Martinez, *J. Phys. Chem. A*, 2009, **113**, 1134.
57 P. Pyykkö, *Adv. Quantum Chem.*, 1978, **11**, 353.
58 P. Pyykkö and J. P. Desclaux, *Acc. Chem. Res.*, 1979, **12**, 276.
59 P. Pyykkö, *Chem. Rev.*, 1988, **88**, 563.
60 H. Häkkinen, M. Moseler and U. Landman, *Phys. Rev. Lett.*, 2002, **89**, 33401.
61 H. Haekkinen, B. Yoon, U. Landman, X. Li, H. Zhai and L. Wang, *J. Phys. Chem. A*, 2003, **107**, 6168.
62 X.-G. Xiong, W.-H. Xu, J. Li and P. Pyykkö, *Int. J. Mass Spectrom.*, 2013, **354–355**, 15.
63 S. Grimme, *J. Comput. Chem.*, 2006, **27**, 1787.
64 S. Grimme, J. Antony, S. Ehrlich and H. Krieg, *J. Chem. Phys.*, 2010, **132**, 154104.
65 M. Seth and T. Ziegler, *J. Chem. Theory Comput.*, 2012, **8**, 901.
66 A. Bondi, *J. Phys. Chem.*, 1964, **68**, 441.
67 R. S. Rowland and R. Taylor, *J. Phys. Chem.*, 1996, **100**, 7384.
68 E. S. Kryachko, *J. Mol. Struct.*, 2008, **880**, 23.
69 E. S. Kryachko and F. Remacle, *Chem. Phys. Lett.*, 2005, **404**, 142.
70 E. S. Kryachko, A. Karpfen and F. Remacle, *J. Phys. Chem. A*, 2005, **109**, 7309.
71 E. S. Kryachko and F. Remacle, *J. Chem. Phys.*, 2007, **127**, 194305.
72 E. Arunan, G. R. Desiraju, R. A. Klein, J. Sadlej, S. Scheiner, I. Alkorta, D. C. Clary, R. H. Crabtree, J. J. Dannenberg, P. Hobza, H. G. Kjaergaard, A. C. Legon, B. Mennucci and D. J. Nesbitt, *Pure Appl. Chem.*, 2011, **83**, 1637.
73 U. Koch and P. L. A. Popelier, *J. Phys. Chem.*, 1995, **99**, 9747.
74 P. L. A. Popelier, *J. Phys. Chem. A*, 1998, **102**, 1873.
75 K. B. Wiberg, R. F. W. Bader and C. D. H. Lau, *J. Am. Chem. Soc.*, 1987, **109**, 1001.